Global airborne sampling reveals a previously unobserved dimethyl sulfide oxidation mechanism in the marine atmosphere

Patrick R. Veres[a,1], J. Andrew Neuman[a,b], Timothy H. Bertram[c], Emmanuel Assaf[a,b], Glenn M. Wolfe[d,e], Christina J. Williamson[a,b], Bernadett Weinzierl[f], Simone Tilmes[g], Chelsea R. Thompson[a,b], Alexander B. Thames[h], Jason C. Schroder[b,i,2], Alfonso Saiz-Lopez[j], Andrew W. Rollins[a], James M. Roberts[a], Derek Price[b,i], Jeff Peischl[a,b], Benjamin A. Nault[b,i], Kristian H. Møller[k], David O. Miller[h], Simone Meinardi[l], Qinyi Li[j], Jean-François Lamarque[m], Agnieszka Kupc[a,b,f], Henrik G. Kjaergaard[k], Douglas Kinnison[g], Jose L. Jimenez[b,i], Christopher M. Jernigan[c], Rebecca S. Hornbrook[g], Alan Hills[g], Maximilian Dollner[f], Douglas A. Day[b,i], Carlos A. Cuevas[j], Pedro Campuzano-Jost[b,i], James Burkholder[a], T. Paul Bui[n], William H. Brune[h], Steven S. Brown[a], Charles A. Brock[a], Ilann Bourgeois[a,b], Donald R. Blake[l], Eric C. Apel[g], and Thomas B. Ryerson[a]

[a]Chemical Sciences Division, Earth System Research Laboratory, National Oceanic and Atmospheric Administration, Boulder, CO 80305; [b]Cooperative Institute for Research in Environmental Sciences, University of Colorado Boulder, Boulder, CO 80309; [c]Department of Chemistry, University of Wisconsin–Madison, Madison, WI 53706; [d]Atmospheric Chemistry and Dynamics Laboratory, NASA Goddard Space Flight Center, Greenbelt, MD 20771; [e]Joint Center for Earth Systems Technology, University of Maryland, Baltimore County, Baltimore, MD 21250; [f]Faculty of Physics, Aerosol Physics and Environmental Physics, University of Vienna, 1090 Vienna, Austria; [g]Atmospheric Chemistry Observations & Modeling Laboratory, National Center for Atmospheric Research, Boulder, CO 80301; [h]Department of Meteorology and Atmospheric Science, Pennsylvania State University, University Park, PA 16801; [i]Department of Chemistry, University of Colorado Boulder, Boulder, CO 80309; [j]Department of Atmospheric Chemistry and Climate, Institute of Physical Chemistry Rocasolano, Consejo Superior de Investigaciones Científicas, 28006 Madrid, Spain; [k]Department of Chemistry, University of Copenhagen, 1165 Copenhagen, Denmark; [l]School of Physical Science, University of California, Los Angeles, CA 90095; [m]Climate & Global Dynamics Lab, National Center for Atmospheric Research, Boulder, CO 80301; and [n]Ames Research Center, NASA, Mountain View, CA 94043

Edited by John H. Seinfeld, California Institute of Technology, Pasadena, CA, and approved January 21, 2020 (received for review November 5, 2019)

Dimethyl sulfide (DMS), emitted from the oceans, is the most abundant biological source of sulfur to the marine atmosphere. Atmospheric DMS is oxidized to condensable products that form secondary aerosols that affect Earth's radiative balance by scattering solar radiation and serving as cloud condensation nuclei. We report the atmospheric discovery of a previously unquantified DMS oxidation product, hydroperoxymethyl thioformate (HPMTF, $HOOCH_2SCHO$), identified through global-scale airborne observations that demonstrate it to be a major reservoir of marine sulfur. Observationally constrained model results show that more than 30% of oceanic DMS emitted to the atmosphere forms HPMTF. Coincident particle measurements suggest a strong link between HPMTF concentration and new particle formation and growth. Analyses of these observations show that HPMTF chemistry must be included in atmospheric models to improve representation of key linkages between the biogeochemistry of the ocean, marine aerosol formation and growth, and their combined effects on climate.

dimethyl sulfide | marine sulfur | autoxidation | marine aerosols | aerosol sulfate

Dimethyl sulfide (DMS; CH_3SCH_3) is naturally emitted from the oceans and is the most abundant biological source of sulfur to the marine atmosphere (1–3). DMS is produced from a variety of marine phytoplankton and readily partitions to the atmosphere where it undergoes radical-initiated oxidation by hydroxyl (OH), halogen radicals (e.g., chlorine [Cl] and bromine oxide [BrO]), and the nitrate radical (NO_3) to form sulfur dioxide (SO_2) and methane sulfonic acid (MSA; CH_3SO_3H), according to traditional descriptions of DMS oxidation chemistry (1, 2, 4–7). Gas-phase SO_2 can be oxidized further to form sulfuric acid (H_2SO_4), a key precursor to new particles formed via homogeneous nucleation in air masses where the existing condensation sink is small (8). These newly formed particles may grow by further condensation and coagulation to sizes large enough to serve as cloud condensation nuclei (CCN), thus affecting cloud optical properties and climate (9). In addition, SO_2 can partition to aerosol liquid water to form non-sea salt sulfate ($nss\text{-}SO_4^{2-}$) (10). Gas-phase MSA contributes to particle growth via condensation onto existing particles (11).

Studies of DMS oxidation have focused almost exclusively on the fate of the terminal products SO_2 and MSA and their impact

Significance

Dimethyl sulfide (DMS) has been the subject of a decades-long research effort due to its role as the major natural global sulfur emission. DMS oxidation across the world's ocean basins is thought to produce sulfate aerosol, which in turn alters Earth's albedo and climate. Details of the DMS oxidation mechanism are critical in defining this atmospheric chemistry–climate interaction. We present the atmospheric discovery and global in situ observations of a major DMS gas-phase oxidation product, hydroperoxymethyl thioformate (HPMTF). Inclusion of HPMTF in descriptions of DMS oxidation is essential in models addressing marine aerosol formation, growth, and global distributions of cloud condensation nuclei (CCN). These findings represent a major shift in the understanding of this important biogeochemical cycle.

Author contributions: P.R.V. designed research; P.R.V., J.A.N., T.H.B., C.J.W., B.W., S.T., C.R.T., A.B.T., J.C.S., A.W.R., D.P., J.P., B.A.N., D.O.M., S.M., A.K., J.L.J., R.S.H., A.H., M.D., D.A.D., P.C.-J., T.P.B., W.H.B., C.A.B., I.B., D.R.B., E.C.A., and T.B.R. performed research; P.R.V., E.A., G.M.W., A.S.-L., J.M.R., K.H.M., Q.L., J.-F.L., H.G.K., D.K., C.M.J., C.A.C., J.B., and S.S.B. contributed new reagents/analytic tools; P.R.V., J.A.N., T.H.B., C.J.W., B.W., S.T., C.R.T., A.B.T., J.C.S., A.S.-L., A.W.R., D.P., J.P., B.A.N., K.H.M., D.O.M., S.M., Q.L., A.K., H.G.K., J.L.J., C.M.J., R.S.H., A.H., M.D., D.A.D., P.C.-J., T.P.B., W.H.B., C.A.B., I.B., D.R.B., E.C.A., and T.B.R. analyzed data; and P.R.V., J.A.N., T.H.B., and S.S.B. wrote the paper.

The authors declare no competing interest.

This article is a PNAS Direct Submission.

Data deposition: Iodide chemical ionization time-of-flight mass spectrometer laboratory calibration data are available at Figshare, https://figshare.com/articles/PNAS_HPMTF_Laboratory_Calibration_Data/11538789/2. The NASA Atom dataset is available at Oak Ridge National Laboratory Distributed Active Archive Center, https://daac.ornl.gov/cgi-bin/dsviewer.pl?ds_id=1581.

[1]To whom correspondence may be addressed. Email: patrick.veres@noaa.gov.

[2]Present address: Air Pollution Control Division, Colorado Department of Public Health and Environment, Denver, CO 80246.

This article contains supporting information online at https://www.pnas.org/lookup/suppl/doi:10.1073/pnas.1919344117/-/DCSupplemental.

First published February 18, 2020.

on the concentration of CCN (9). Many of the proposed intermediates in the complex DMS oxidation scheme have not been directly observed, thus creating uncertainty in the DMS product branching ratios and oxidation timescales. For example, current estimates of the global fraction of DMS that is oxidized to SO_2 range from 0.15 to 1 (4, 6, 12), highlighting the large variability of DMS oxidation chemistry in existing models. Accurate representation of both the DMS oxidation product branching ratios and timescales in chemical transport models is critical to establishing a relationship between oceanic DMS emissions, atmospheric particle number and mass concentrations, and CCN concentrations in the marine boundary layer (MBL) relative to other sources of marine CCN, such as sea spray aerosol, long-range transport of terrestrial particles, and secondary marine aerosol produced from non-DMS precursors (7, 13, 14), in both preindustrial and present-day atmospheres (15).

Here we present atmospheric observations of a newly discovered stable intermediate in the DMS oxidation process, hydroperoxymethyl thioformate (HPMTF; $HOOCH_2SCHO$). HPMTF is formed from the methylthiomethylperoxy radical ($CH_3SCH_2OO\bullet$), the primary product of the hydrogen abstraction (H abstraction) reaction of OH with DMS, through subsequent unimolecular hydrogen shifts (H shifts), a process that was initially theoretically proposed (16) and more recently validated in a laboratory study (17). HPMTF has not been previously reported in the atmosphere and therefore has not been widely incorporated into atmospheric models describing sulfur oxidation in the remote marine atmosphere. Our global-scale airborne in situ observations of HPMTF, made during the NASA Atmospheric Tomography (ATom) mission, show that HPMTF is a major reservoir of marine sulfur.

The ATom mission used the instrumented NASA DC-8 research aircraft between 2016 and 2018 to sample the daytime atmosphere in four global circuits, from the Arctic to the Antarctic over the remote Pacific and Atlantic Oceans (Fig. 1) (18). A new iodide-ion chemical ionization time-of-flight mass spectrometer (iodide CIMS) (19) was added to the payload for the ATom-3 (September to October 2017) and ATom-4 (April to May 2018) global circuits, when over 150 vertical profiles were conducted from 0.2 to 14 km above the ocean surface between 80°N and 85°S latitudes. The iodide CIMS detected a previously unobserved organic sulfur species, $C_2H_4O_3S$, enhanced in the remote marine atmosphere. We developed analytical techniques, including in situ isotopic labeling during ATom-4, and a chemical formation mechanism to identify $C_2H_4O_3S$ as HPMTF, a product of DMS oxidation. Subsequent laboratory generation and quantification of HPMTF confirmed the molecular structure and established absolute atmospheric abundances. Detection limits were better than 1 parts per trillion as a mole fraction in dry air (ppt), with an uncertainty of 55% + 0.06 ppt and a precision of 0.1 ppt for 1-s measurements (details in *SI Appendix*).

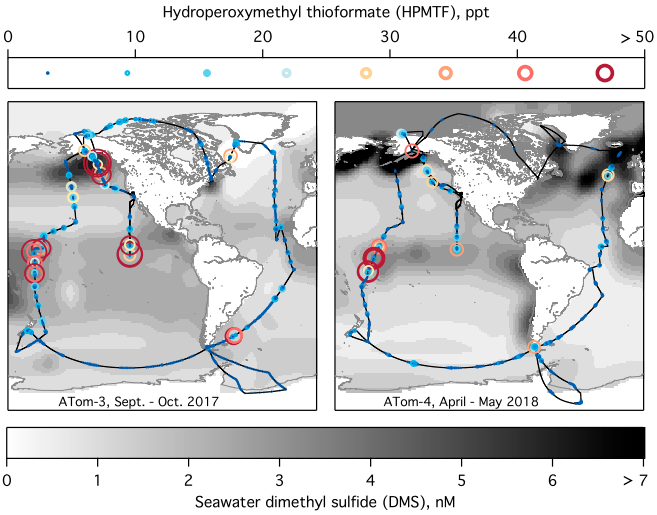

Fig. 1. Measurements of HPMTF during the ATom mission. NASA DC-8 flight tracks are colored and sized by atmospheric mixing ratios of HPMTF observed during ATom-3 and ATom-4, displayed as 5-min averages of observations above the 0.1-ppt detection limit. Climatological surface seawater DMS concentrations are shown on a grayscale (20).

In situ HPMTF observations in the lower troposphere and MBL along the ATom-3 and ATom-4 flight tracks, along with monthly averaged DMS seawater climatology from Lana et al. (20), are shown in Fig. 1. There are three salient features of the ATom HPMTF dataset: 1) HPMTF mixing ratios are largest in the MBL in regions where seawater DMS concentrations, and thus atmospheric DMS emissions, are expected to be the greatest (Fig. 1); 2) HPMTF is globally ubiquitous in the lower atmosphere over both seasons sampled, with MBL mixing ratios frequently exceeding 50 ppt and periodically as large as several hundred ppt (Fig. 2); and 3) average HPMTF mixing ratios in the middle to upper troposphere are generally below the 0.1-ppt instrumental detection limit.

ATom observations of HPMTF, DMS, and SO_2 are summarized in Fig. 2 for periods where observations exceed instrumental detection limits. Vertically resolved, globally averaged DMS, SO_2, and HPMTF mixing ratios show similar behavior throughout the troposphere (*SI Appendix*, Fig. S2 *E* and *F*) with the largest enhancements observed at the lowest altitudes. HPMTF was typically observed in a 1:1 ratio with DMS in the MBL; however, values in excess of 2:1 were frequently encountered. For example, the largest HPMTF mixing ratios of more than 300 ppt were observed over the South Atlantic Ocean (46°S and 53°W) during ATom-3 and corresponded to the maximum in observed DMS of more than 120 ppt. Comparing HPMTF to DMS and SO_2 concentrations reveals that HPMTF is a major reservoir of marine sulfur.

HPMTF mixing ratios decreased abruptly in cloud, identified using cloud aerosol probes, often approaching the detection limit (Fig. 3). This response indicates that uptake on aqueous cloud particles is rapid and may partially explain the variability in the relationship between HPMTF and sea surface DMS (Fig. 1). On average, a 75% reduction in HPMTF abundance within the MBL was observed in the presence of clouds during ATom-3 and ATom-4, while DMS mixing ratios varied by a maximum of 25% between cloudy and clear conditions. Loss of HPMTF via aqueous uptake to clouds or the ocean surface is therefore expected to play a role in the atmospheric lifetime and processing of MBL sulfur. Aqueous uptake may lead to the formation of oxidized sulfur products, such as SO_2, sulfur trioxide (SO_3), or sulfate (SO_4^{2-}).

Coincident aerosol mass and submicron aerosol composition measurements during ATom indicate a link between HPMTF abundance and the mass of submicron sulfate (*SI Appendix*, Fig. S1). MBL enhancements in HPMTF are at times associated with MSA abundance in submicron aerosol (*SI Appendix*, Fig. S2*A*). However, generally, there is no apparent relationship between gas-phase mixing ratios of HPMTF and particulate MSA concentrations when all observations from the ATom-3 and ATom-4 are considered (*SI Appendix*, Fig. S2*B*).

Fig. 4 illustrates the relationship between HPMTF and particulate number concentration where newly formed particles (peak mean diameter of ~20 nm) were observed over the northern Atlantic Ocean. Enhancements in particle number concentration for the smallest observable sizes (3 to 10 nm) are associated with enhancements in HPMTF just above clouds at the top of the MBL. These observations are consistent with DMS oxidation-driven particle formation or growth. However, with airborne observations it is difficult to definitively state the age or source of these nucleation mode particles. Previously reported observations

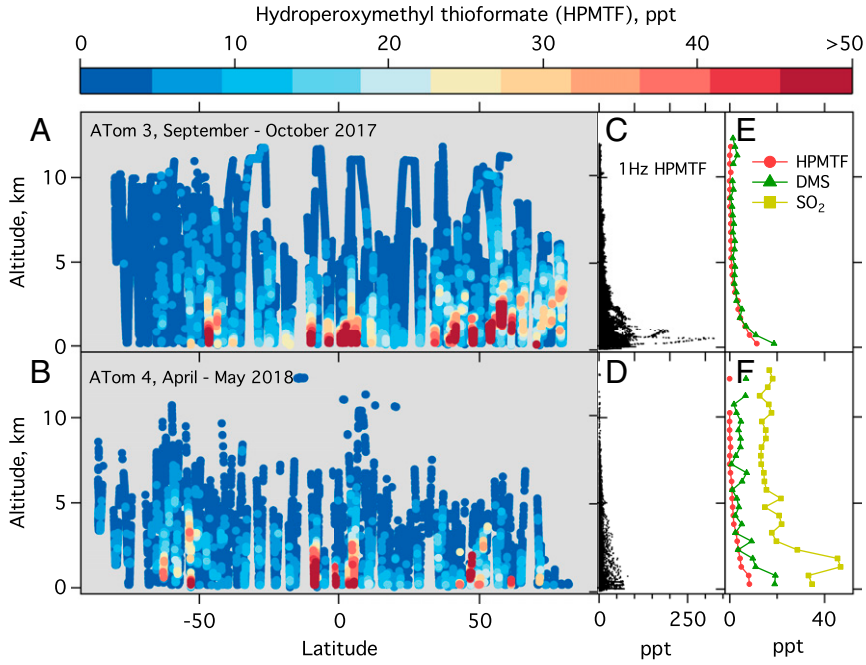

Fig. 2. Global observations of HPMTF from ATom-3 and ATom-4. (*A* and *B*) Global observations of HPMTF made aboard the NASA DC-8 aircraft during the ATom-3 and ATom-4 circuits. The 1-Hz observations of HPMTF are colored according to the legend above. (*C* and *D*) Vertical distribution of all HPMTF 1-Hz observations. (*E* and *F*) HPMTF, DMS, and SO_2 vertically binned (0.5 km resolution) mean observations. HPMTF, SO_2, and DMS observations below the detection limit of the instrument were not included in the data presented.

of similar particle formation and growth events above the MBL where existing particle surface area was small, were attributed to DMS oxidation to SO_2 leading to sulfuric acid nucleation (21–23). Our observations suggest that HPMTF may contribute to particle formation and growth events in cloud outflow; however, estimates of HPMTF-driven particle formation relative to other sulfur species cannot be determined from the ATom observations alone.

We propose that HPMTF formation plays a substantial role in sulfate particle formation and/or growth from DMS oxidation, either directly or via its impact on SO_2 formation yields. One or more of the following scenarios may explain the correlation of HPMTF with SO_2, particulate MSA, and submicron aerosol sulfate (SO_4^{2-}): 1) HPMTF is coproduced with lower-volatility oxidation products such as MSA, 2) HPMTF can be oxidized to SO_2 with subsequent gas-phase H_2SO_4 and SO_4^{2-} production, or 3) HPMTF may be oxidized in the gaseous or condensed phase to directly contribute to the growth of existing aerosol.

The relationships observed between HPMTF, DMS, SO_2, and SO_4^{2-} strongly suggest that HPMTF is formed by DMS oxidation, a conclusion that is supported by recent theoretical and laboratory oxidation studies that identify $HOOCH_2SCHO$ as a product of DMS autoxidation (16, 17). Production of HPMTF in the atmosphere is initiated by the H abstraction reaction of OH with DMS and subsequent molecular oxygen (O_2) addition to produce the methylthioxymethyl-peroxy radical ($CH_3SCH_2OO\bullet$).

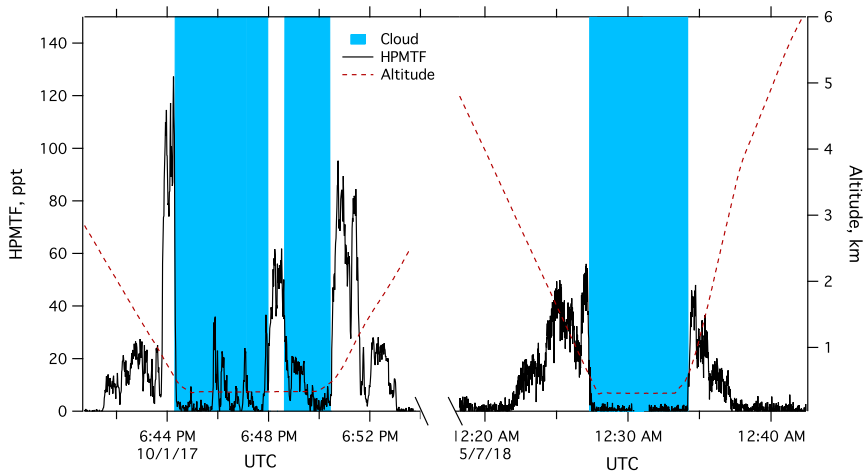

Fig. 3. Example time series of HPMTF removal by cloud uptake. In situ observations of HPMTF during ATom-3 and ATom-4 (black) are strongly anticorrelated with observed clouds (blue). Observations over the northern Atlantic Ocean (47°N and 135°W; *Left*) and the South Pacific Ocean (62°S and 150°W; *Right*) show similar a similar response to clouds suggesting that cloud removal of HPMTF is a dominant atmospheric loss process.

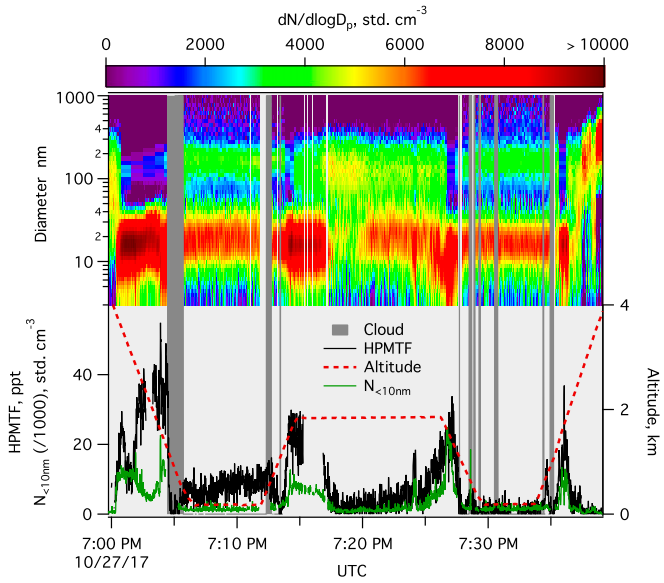

Fig. 4. Evidence for DMS oxidation-driven particle formation and growth. In situ measurements made over the northern Atlantic Ocean (47°N and 135°W) of particle size and number concentration at altitudes of 1 to 3 km, above the MBL (*Top*), are strongly correlated with HPMTF mixing ratios (*Bottom*; black). A time series of total particle number for the size range below 10 nm is included in *Bottom* (green) to highlight the correlation between HPMTF and particles in the smallest size range observed. Cloud observations are indicated by the shaded regions (gray).

$CH_3SCH_2OO\bullet$ can undergo a rapid unimolecular H shift to form $\bullet CH_2SCH_2OOH$. Then, molecular O_2 addition and an additional rapid H shift, a process known as autoxidation (24), produces HPMTF and regenerates OH. Consideration of this HPMTF formation mechanism in standard models of DMS oxidation reduces SO_2 yields (5) and may have a substantial effect on lifetime and distribution of marine sulfur species.

The ATom observations provide constraints on the importance of HPMTF formation relative to other oxidation pathways and enable the development of an accurate chemical mechanism. We developed a model to constrain branching ratios for the DMS oxidation processes identified in Fig. 5 utilizing ATom measurements of the primary atmospheric DMS gas-phase oxidants (OH and BrO) combined with known kinetic data (details provided in *SI Appendix*, section 4). In the model, H abstraction accounts for 40 to 50% of the instantaneous DMS loss rate in the lowest 2 km of the atmosphere where DMS is most abundant, leading to the formation of $CH_3SCH_2OO\bullet$. The relative importance of the OH abstraction reaction decreases to less than 20% at altitudes above 8 km (*SI Appendix*, Fig. S3*B*). The OH addition channel to produce MSA accounts for another 40 to 50%. Counter to previous studies (4, 5), we find that BrO contributes less than 5% to the instantaneous DMS loss rate due to the relatively lower BrO mixing ratios observed here. ATom observations show that over the remote oceans below 2 km altitude, BrO mixing ratios averaged 0.1 ppt, with a measurement uncertainty of 25% + 0.2 ppt. Nighttime DMS oxidation via NO_3 radical is not considered in this study but would proceed through the same peroxy radical intermediate and has been shown to contribute significantly to DMS oxidation (4, 25, 26). The low concentrations of NO expected in the nighttime atmosphere would further increase the yield of HPMTF relative to SO_2 and are therefore also expected to play a role in HPMTF formation.

Our model results show that once formed, the fate of $CH_3SCH_2OO\bullet$ depends on the competition between isomerization to $\bullet CH_2SCH_2OOH$ and reaction with hydroperoxyl radical (HO_2) and nitric oxide (NO). The estimated first-order rate of 2.1 s^{-1} at 293 K for the first H shift in $CH_3SCH_2OO\bullet$ (16) and the rate recently determined from laboratory kinetic studies, 0.23 s^{-1} at 295 K (17), are considerably greater than experimental and calculated autoxidation rates for analogous peroxy radicals (24, 27, 28). Using the multiconformer transition state theory (MC-TST) approach of Møller et al. (27) (see *SI Appendix*, section 5, for details), which has shown good agreement with experimentally determined H shift rate coefficients (29), we calculate the first (and rate-limiting) H shift rate to be significantly slower (0.041 s^{-1} at 293 K) than previously determined (16). Despite this reduction in the calculated H shift rate, the rate remains four times faster than the bimolecular reaction of $CH_3SCH_2OO\bullet$ with HO_2 and NO in the global remote daytime MBL for typical ATom conditions (*SI Appendix*, Fig. S3*C*).

The contributions of each oxidation pathway of DMS removal were estimated using gas-phase kinetic calculations constrained by these revised theoretical H shift rates (0.021 s^{-1} at 284 K and

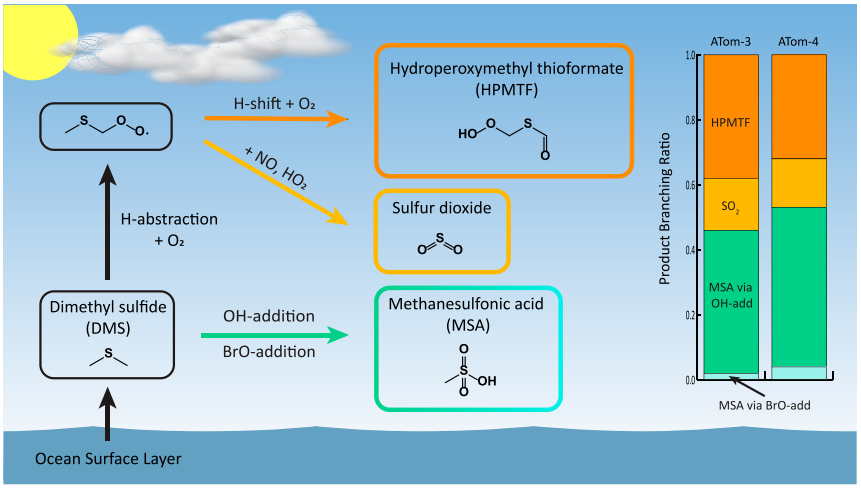

Fig. 5. Observationally constrained DMS oxidation mechanism. Updated DMS oxidation scheme containing the HPMTF formation pathway. This work assumes that DMS addition reactions (BrO and OH) ultimately form MSA, while bimolecular oxidation via NO or HO_2 yields SO_2, a simplified model based on traditional descriptions of DMS oxidation (5). Product branching ratios for the four reaction pathways are shown as a stacked bar graph. Calculated ratios are constrained by mean ATom measurements for OH, HO_2, NO, BrO, and temperature for daytime solar zenith angles <75° and altitude <2 km.

0.028 s^{-1} at 288 K) and ATom-3 and ATom-4 observations of OH, BrO, NO, and HO_2 (*SI Appendix*, Fig. S3*A*). We have chosen to use the slowest estimate of the H shift rate to present the most conservative assessment of the inclusion of this chemistry to the DMS oxidation scheme. If the rate of the rate-limiting H shift is faster than our calculated value as suggested by recent experiments (23), then this chemistry becomes even more important in the atmosphere. In this analysis, the OH and BrO addition channels are assumed to yield MSA as a terminal product, a simplification based on current traditional descriptions of DMS oxidation (5). In the remote atmosphere below 2 km, the model results show that ∼60% of the intermediate $CH_3SCH_2OO\bullet$ reacts via autoxidation to form HPMTF, with the remainder assumed to yield SO_2. The difference between modeled ATom-3 and ATom-4 HPMTF yields of 0.38 (288.4 K) and 0.32 (283.6 K), respectively, reflects a change in average observed temperatures with lower temperatures favoring OH addition, which does not lead to HPMTF formation, over H abstraction (30) and subsequent autoxidation. These observationally constrained model results indicate that more than 30% of atmospheric DMS is oxidized to HPMTF. This result corresponds to an ∼60% reduction in the yield of prompt SO_2 formation from DMS oxidation.

In order to examine the potential impact of this chemistry on the global marine atmosphere, HPMTF formation from DMS oxidation was also implemented in a global chemical transport model [CAM-chem (31)] using the temperature-dependent H shift rate coefficient reported here. The lack of knowledge of the atmospheric fate of HPMTF is a limitation of these simulations, where gas-phase oxidation by OH is assumed to be the sole sink for HPMTF in the model with an approximated rate coefficient of 1.4×10^{-12} cm^3 $molecule^{-1}$ s^{-1} (16). CAM-chem model simulations, with and without the autoxidation mechanism, were used to estimate the potential influence of HPMTF chemistry on SO_2 and sulfate production (*SI Appendix*, Table S1). Addition of the HPMTF oxidation pathway to the CAM-chem model slows DMS oxidation to SO_2 reducing the SO_2 and SO_4^{2-} abundance at the surface in areas where DMS is emitted, ∼60°N to 60°S. The modeled difference is up to 50% net reduction in SO_2 and 30% in SO_4^{2-} at the surface (*SI Appendix*, Fig. S4). This difference is substantial but represents an upper limit in reduction because oxidation of HPMTF by aqueous and heterogeneous processes may also lead to SO_2 and SO_4^{2-} production and compensate for this reduction. Unreacted sulfur species produced after DMS oxidation, prior to forming SO_2 (e.g., HPMTF [*SI Appendix*, Fig. S5]), can reach the polar regions and continue oxidizing to produce additional SO_2 and sulfate (*SI Appendix*, Fig. S4). These simulated polar enhancements are considered upper limits due to a lack of inclusion of accurate HPMTF loss processes in the model, which are currently unknown. Nonetheless, the magnitude of the changes observed in these global model simulations highlight the potential impact of this sulfur chemistry in reshaping the spatial distribution and abundance of marine sulfur species (i.e., HPMTF, SO_2, and sulfate).

The expected response of aerosol particle and CCN concentrations to changes in DMS emissions depends strongly on the rate of formation and fate of HPMTF. For example, if the primary product of further HPMTF oxidation is through a gas-phase mechanism to produce SO_2, the effect on the marine sulfur budget relative to current understanding would be small. By contrast, prompt oxidation of HPMTF to nss-SO_4^{2-} would increase the rate of formation of condensed phase sulfate. In this case, a change in DMS emissions in response to climate change (32) would readily perturb aerosol sulfate and may introduce an important feedback. Furthermore, since DMS emission rates, the competition between OH addition and H abstraction, and the rate of the autoxidation reaction are temperature-dependent, the abundance and speciation of DMS oxidation products may be sensitive to climate change and provide a climate feedback. Determination of the gas- and condensed-phase chemistry of HPMTF is therefore needed to improve model simulations of marine sulfur chemistry and assess the potential impact on radiative forcing. This discovery of HPMTF over the remote oceans may necessitate a reevaluation of several decades of research assessing the role of DMS in marine sulfur chemistry and its impact on new particle formation and growth, the global distribution of CCN, and their effects on Earth's radiative balance.

Methods and Materials

Details on the operation, data analysis, and calibration procedure for the iodide CIMS instrument used to measure HPMTF are provided in *SI Appendix*, section 1. Descriptions of the supplemental gas-phase measurement techniques are provided in *SI Appendix*, section 2. Particle composition and size measurement techniques are described in detail in *SI Appendix*, section 3. Details on the kinetic calculations used to produce Fig. 5, the MC-TST approach, and the CAM-chem global model simulations are provided in *SI Appendix*.

Data Availability. ATom data used in this study are published through the Distributed Active Archive Center for Biogeochemical Dynamics (18). Iodide CIMS laboratory calibration data that were used in this study have been published as a dataset (33).

ACKNOWLEDGMENTS. We thank the ATom leadership team, science team, and crew for contributions to the ATom measurements. Additional National Oceanic and Atmospheric Administration (NOAA) support for ATom was provided by NASA funding via Inter-Agency Transfer NNH15AB12I and by funding from the NOAA Climate Program Office and the NOAA Atmospheric Chemistry, Carbon Cycle, and Climate program. K.H.M. and H.G.K. acknowledge the financial support of the Independent Research Fund Denmark, the University of Copenhagen, and the Danish Ministry for Higher Education and Science's Elite Research travel grant. J.L.J.'s group acknowledges NASA grants NHX15AH33A and 80NSSC19K0124. A.K. was supported by the Austrian Science Fund's Erwin Schrodinger Fellowship. A.S.-L., Q.L., and C.A.C. are supported by the European Research Council (ERC) Executive Agency under the European Union's Horizon 2020 Research and Innovation programme (Project ERC-2016-COG 726349 CLIMAHAL). The National Center for Atmospheric Research is sponsored by the National Science Foundation. E.A. and J.B. were funded in part by NASA Atmospheric Composition Program. T.H.B. and C.M.J. acknowledge support from the National Science Foundation Center for Aerosol Impacts on Chemistry of the Environment under grant CHE 1801971. B.W. and M.D. have received funding from the ERC under the European Union's Horizon 2020 research and innovation framework program under grant 640458 (A-LIFE) and from the University of Vienna.

1. M. O. Andreae *et al*., Dimethyl sulfide in the marine atmosphere. *J. Geophys. Res.* **90**, 2891–2900 (1985).
2. M. O. Andreae, Ocean-atmosphere interactions in the global biogeochemical sulfur cycle. *Mar. Chem.* **30**, 1–29 (1990).
3. T. S. Bates, B. K. Lamb, A. Guenther, J. Dignon, R. E. Stoiber, Sulfur emissions to the atmosphere from natural sources. *J. Atmos. Chem.* **14**, 315–337 (1992).
4. Q. J. Chen, T. Sherwen, M. Evans, B. Alexander, DMS oxidation and sulfur aerosol formation in the marine troposphere: A focus on reactive halogen and multiphase chemistry. *Atmos. Chem. Phys.* **18**, 13617–13637 (2018).
5. E. H. Hoffmann *et al*., An advanced modeling study on the impacts and atmospheric implications of multiphase dimethyl sulfide chemistry. *Proc. Natl. Acad. Sci. U.S.A.* **113**, 11776–11781 (2016).
6. I. Faloona, Sulfur processing in the marine atmospheric boundary layer: A review and critical assessment of modeling uncertainties. *Atmos. Environ.* **43**, 2841–2854 (2009).
7. P. K. Quinn, T. S. Bates, The case against climate regulation via oceanic phytoplankton sulphur emissions. *Nature* **480**, 51–56 (2011).
8. M. Kulmala, Atmospheric science. How particles nucleate and grow. *Science* **302**, 1000–1001 (2003).
9. J. Merikanto, D. V. Spracklen, G. W. Mann, S. J. Pickering, K. S. Carslaw, Impact of nucleation on global CCN. *Atmos. Chem. Phys.* **9**, 8601–8616 (2009).
10. J. Boniface *et al*., Uptake of gas-phase SO2, H2S, and CO2 by aqueous solutions. *J. Phys. Chem. A* **104**, 7502–7510 (2000).
11. E. S. Saltzman, D. L. Savoie, R. G. Zika, J. M. Prospero, Methane sulfonic-acid in the marine atmosphere. *J. Geophys. Res.* **88**, 897–902 (1983).
12. T. Berndt, S. Richters, Products of the reaction of OH radicals with dimethyl sulphide in the absence of NOx: Experiment and simulation. *Atmos. Environ.* **47**, 316–322 (2012).
13. C. D. O'Dowd, G. De Leeuw, Marine aerosol production: A review of the current knowledge. *Philos. Trans. R. Soc. A* **365**, 1753–1774 (2007).
14. K. A. Prather *et al*., Bringing the ocean into the laboratory to probe the chemical complexity of sea spray aerosol. *Proc. Natl. Acad. Sci. U.S.A.* **110**, 7550–7555 (2013).

15. K. S. Carslaw *et al*., Large contribution of natural aerosols to uncertainty in indirect forcing. *Nature* **503**, 67–71 (2013).
16. R. Wu, S. Wang, L. Wang, New mechanism for the atmospheric oxidation of dimethyl sulfide. The importance of intramolecular hydrogen shift in a CH_3SCH_2OO radical. *J. Phys. Chem. A* **119**, 112–117 (2015).
17. T. Berndt *et al*., Fast peroxy radical isomerization and OH recycling in the reaction of OH radicals with dimethyl sulfide. *J. Phys. Chem. Lett.* **10**, 6478–6483 (2019).
18. S. C. Wofsy *et al*., *ATom: Merged Atmospheric Chemistry, Trace Gases, and Aerosols* (Oak Ridge National Laboratory Distributed Active Archive Center, 2018). https://daac.ornl.gov/cgi-bin/dsviewer.pl?ds_id=1581. Accessed 29 November 2019.
19. B. H. Lee *et al*., An iodide-adduct high-resolution time-of-flight chemical-ionization mass spectrometer: Application to atmospheric inorganic and organic compounds. *Environ. Sci. Technol.* **48**, 6309–6317 (2014).
20. A. Lana *et al*., An updated climatology of surface dimethlysulfide concentrations and emission fluxes in the global ocean. *Global Biogeochem. Cycles* **25**, GB1004 (2011).
21. A. D. Clarke, Z. Li, M. Litchy, Aerosol dynamics in the equatorial Pacific Marine boundary layer: Microphysics, diurnal cycles and entrainment. *Geophys. Res. Lett.* **23**, 733–736 (1996).
22. A. D. Clarke *et al*., Particle production in the remote marine atmosphere: Cloud outflow and subsidence during ACE 1. *J. Geophys. Res.* **103**, 16397–16409 (1998).
23. M. de Reus *et al*., Aerosol production and growth in the upper free troposphere. *J. Geophys. Res.* **105**, 24751–24762 (2000).
24. J. D. Crounse, L. B. Nielsen, S. Jorgensen, H. G. Kjaergaard, P. O. Wennberg, Autoxidation of organic compounds in the atmosphere. *J. Phys. Chem. Lett.* **4**, 3513–3520 (2013).
25. N. R. Jensen, J. Hjorth, C. Lohse, H. Skov, G. Restelli, Products and mechanisms of the gas-phase reactions of NO3 with CH3SCH3, CD3SCD3, CH3SH and CH3SSCH3. *J. Atmos. Chem.* **14**, 95–108 (1992).
26. H. Stark *et al*., Influence of nitrate radical on the oxidation of dimethyl sulfide in a polluted marine environment. *J. Geophys. Res.* **112**, 11 (2007).
27. K. H. Møller, R. V. Otkjær, N. Hyttinen, T. Kurtén, H. G. Kjaergaard, Cost-effective implementation of multiconformer transition state theory for peroxy radical hydrogen shift reactions. *J. Phys. Chem. A* **120**, 10072–10087 (2016).
28. R. V. Otkjær, H. H. Jakobsen, C. M. Tram, H. G. Kjaergaard, Calculated hydrogen shift rate constants in substituted alkyl peroxy radicals. *J. Phys. Chem. A* **122**, 8665–8673 (2018).
29. K. H. Møller, K. H. Bates, H. G. Kjaergaard, The importance of peroxy radical hydrogen-shift reactions in atmospheric isoprene oxidation. *J. Phys. Chem. A* **123**, 920–932 (2019).
30. J. B. Burkholder *et al*., "Chemical kinetics and photochemical data for use in atmospheric studies" (Evaluation 18, JPL Publication 15-10, Jet Propulsion Laboratory, Pasadena, 2015).
31. C. A. Cuevas *et al*., Rapid increase in atmospheric iodine levels in the North Atlantic since the mid-20th century. *Nat. Commun.* **9**, 1452 (2018).
32. M. Galí, E. Devred, M. Babin, M. Levasseur, Decadal increase in Arctic dimethylsulfide emission. *Proc. Natl. Acad. Sci. U.S.A.* **116**, 19311–19317 (2019).
33. P. Veres, J. A. Neuman, E. Assaf, HPMTF laboratory calibration data. Figshare. https://figshare.com/articles/PNAS_HPMTF_Laboratory_Calibration_Data/11538789/2. Deposited 7 January 2020.